Electronic thermal conductivity measurements in intrinsic graphene

S. Yiğen, V. Tayari, J. O. Island, J. M. Porter, and A. R. Champagne[*]

Department of Physics, Concordia University, Montréal, Québec, Canada H4B 1R6

The electronic thermal conductivity of graphene and two-dimensional Dirac materials is of fundamental interest and can play an important role in the performance of nanoscale devices. We report the electronic thermal conductivity K_e in suspended graphene in the nearly intrinsic regime over a temperature range of 20–300 K. We present a method to extract K_e using two-point dc electron transport at low bias voltages, where the electron and lattice temperatures are decoupled. We find K_e ranging from 0.5 to 11 W/m K over the studied temperature range. The data are consistent with a model in which heat is carried by quasiparticles with the same mean free path and velocity as graphene's charge carriers.

The electronic heat conductivity of graphene K_e describes how charged quasiparticles carry energy as they diffuse in this material. It could also shed light on K_e in other two-dimensional (2D) Dirac systems whose electronic band structure is related to graphene's, such as the surface states of topological insulators.[1] When a hot electron diffuses out of graphene, it cools down the electronic distribution. Thus, measurements of K_e are needed to complement the understanding of the other hot-electron cooling mechanisms in graphene which involve various electron-phonon couplings.[2–11] Measuring and controlling K_e could have applications in the heat management of heavily doped nm-scale devices where K_e can be dominant,[12] and in optimizing graphene's electro-optical properties.[13,14] While there have been several experimental reports of the phononic thermal conductivity K_p in graphene,[13–21] reports of K_e measurements in suspended graphene are lacking. This is because in most regimes K_p is much larger than K_e, which makes it difficult to measure the amount of heat carried by the charged quasiparticles (electron and holes).

We present a carefully calibrated method to extract K_e in graphene using dc electron transport in suspended devices. The accuracy of the method is dependent on high-mobility (annealed) devices. We present data from three different samples which show consistent results. The extracted K_e are compared with calculated values, $K_{e\text{-th}}$, for a diffusing gas of Dirac quasiparticles. The agreement between theory and measurements is quantitative for all three devices over the temperature range (20–300 K) studied. Throughout the text we use T to designate the lattice (cryostat) temperature, and T_e for the average electron temperature in the suspended devices. At very low bias, $|V_B| \lesssim 1$ mV, $T = T_e$. We first describe our samples, second, we present our T_e thermometry, then show how we apply a controlled ΔT using Joule heating, and finally extract K_e from the transport data.

Figures 1(a) and 1(b) show tilted scanning electron microscopy (SEM) images of samples A and B, respectively (see sample C in the Supplemental Material,[22] SM, Fig. S1). We confirmed using optical contrast and Raman spectroscopy that all three samples are single-layer graphene. Sample A is 650 nm long, 675 nm wide, and suspended 140 ± 10 nm above the substrate [atomic force microscopy (AFM) measurement)] which consists of 100 ± 2 nm of SiO_2 (ellipsometry

measurement) on degenerately doped Si which is used as a back-gate electrode. Sample B is 400 nm long, 1.05 μm wide, and suspended 175 ± 10 nm above a 74 ± 2 nm SiO_2 film on Si. To prepare the samples, we used exfoliated graphene, and standard e-beam lithography to define Ti(5 nm)/Au(80 nm) contacts. The samples were suspended with a wet buffered oxide etch (BOE) such that their only thermal connection is to the gold contacts. We annealed the devices using Joule heating *in situ* by flowing a large current in the devices[23] (up to 540, 840, and 837 μA for A, B, and C). Annealing and subsequent measurements were done under high vacuum, 10^{-6} Torr.

Figures 1(c) and 1(d) show dc two-point resistance data, $R = V_B/I$, for samples A and B, respectively, after annealing, versus gate voltage V_G, which controls charge density. From the width of the R maximum at 11 K, we extract a half width at half maximum (HWHM) of 0.45, 0.6, and 0.95 V for samples A, B, C (sample C, Fig. S1). Using a parallel plate model for the gate capacitance of the devices, these HWHMs correspond to an impurity induced charge density[24] of $n^* \approx 1.5$, 1.7, and 2.1×10^{10} cm^{-2}.

The devices were fabricated with large contact areas between the gold electrodes and graphene crystals, 1.1–3 μm^2 per contact, to minimize the contact resistance R_c. An upper bound for R_c can be extracted from the two-point R-V_G curve in Fig. 1(c) by fitting the data (SM,[22] Sec. 2) with the expression[25] $R = R_o + (L/W)(1/n_G e\mu)$, where R_o is the resistance due to neutral scatterers plus R_c, L is the length of the device, W the width, n_G the charge density induced by V_G, μ the mobility, and e the electron's charge. We fit the data at $T = T_e = 100$ K for $(V_G - V_D) > 1.3$ V to avoid the thermal smearing around the Dirac point V_D. The extracted mobility for sample A in the doped regime is $\mu \approx 8.5 \times 10^4$ cm^2/V s at 100 K, and $R_o \approx 682 \pm 53$ and 1135 ± 80 Ω for hole and electron doping, respectively. The difference between hole, R_{o-h} and electron doping, R_{o-e}, is understood as an additional p-n barrier for the electron due to p doping from the gold electrodes.[25] At the Dirac point, we let $R_{o-\text{Dirac}} = (R_{o-h} + R_{o-e})/2 = 908.5$ Ω for sample A. For sample C, we find $R_{o-\text{Dirac}} = 1097$ Ω. We note that $R_{o-\text{Dirac}}$ is much smaller than R of samples A and C, therefore $R_c < R_{o-\text{Dirac}}$ has at most a modest impact on our measurements in these devices. It is not possible to extract R_o for sample B because it enters the ballistic regime away from the Dirac point (doped regime).[26] The contact areas of
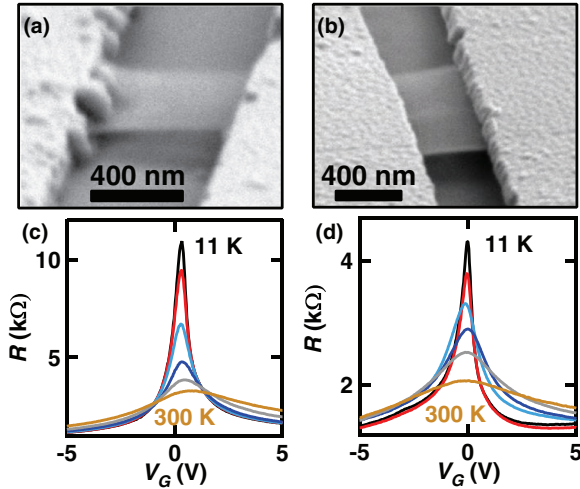
FIG. 1. (Color online) Suspended graphene devices. (a) and (b) Tilted SEM images of 650 and 400 nm long suspended graphene transistors (samples A and B). (c) and (d) R of samples A and B vs gate voltage V_G at $T_e = T = 11$, 50, 100, 150, 210, and 300 K, and $V_B = 0.5$ mV.
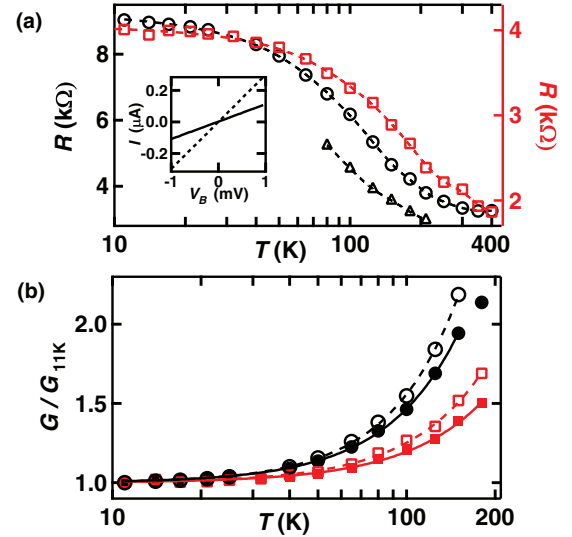

FIG. 2. (Color online) Electron thermometry. (a) Temperature dependence of R in sample A (circles, left axis), sample B (squares, right axis), and sample C (triangles, left axis) near the charge degeneracy $n_G = 5.7, 2.9$ and -1.5×10^9 cm^{-2}. The dashed lines are numerically interpolated curves used for thermometry. Inset: I-V_B data for sample A, $|V_B| < 1$ mV, whose slope is used to extract R. The solid (dashed) line is at $T = T_e = 11$ (300) K. (b) Relative conductance $G/G_{11\,K}$ of sample A (circles) and sample B (squares) vs $T = T_e$. The solid symbols show the raw two-point data, and the open symbols the data after subtracting $R_c = R_{o-\text{Dirac}}$ (see text). The solid and dashed lines are power law fits consistent with charge impurity scattering.

sample B are larger, and its width wider, than for samples A and C. Assuming a similar resistance per unit area as for A and C, we expect $R_c \lesssim 657$ Ω for B. Based on the reported thermal conductance of Au/Ti/graphene and graphene/SiO$_2$ interfaces,[27] the thermal resistance of our contacts are several orders of magnitude lower than the one we measure below for graphene. Thus, the thermal resistance of the contacts can safely be neglected.

Figure 2(a) shows R versus cryostat temperature T calibration curves for samples A (circles, left axis), B (squares, right axis), and C (triangles, left axis) near $V_G = V_D$. $R = V_B/I$ data are extracted from the slope of the I-V_B data as shown in the inset of Fig. 2(a) at 11 K (solid) and 300 K (dashed), for ± 1 mV bias where no Joule heating effect is present ($T_e = T$). The data are taken at $V_G = 0.5$ V close to $V_D = 0.33$ V for sample A, and at $V_G = 0$ V for samples B and C ($V_D = -0.1$ and 0.07 V), corresponding to $n_G = 5.7, 2.9$, and -1.5×10^9 cm^{-2}. The T dependence of the data shows an insulating behavior up to ≈ 200 K for samples A and C, and up to 300 K for sample B. The interpolated dashed lines in Fig. 2(a) will be used as thermometry curves to monitor T_e. Note that the thermometry is most accurate where the curves are steepest.

Figure 2(b) shows the relative conductance $G(T)/G_{11\,K}$ in the intrinsic regime extracted from Fig. 2(a) for samples A and B. The T dependence of G in graphene, at low charge density, is strongly dependent on the type of charge transport. For ballistic transport, we expect a very weak temperature dependence at low T, and a linear dependence when $k_B T \gg E_F$.[28] In the diffusive regime, the expected temperature dependence depends on the type of charge scatterers, and $G(T)/G_{11\,K} \propto T^\alpha$ with $\alpha = -1, 0, 2$ for acoustic phonon, short-range (neutral), and long-range (charged) scatterers, respectively.[11,29] The temperature dependence of real samples is expected to combine all three types of scattering. We fit the data with a function $G/G_{11\,K} = 1 + AT^p$, and extract

$p = 1.85, 1.74, 1.72$, and 1.63 ± 0.03 for sample A with $R_c = R_{o-\text{Dirac}}$ and 0 (open and solid circles), and sample B with $R_c = 657$ and 0 Ω (open and solid squares). This T dependence strongly supports diffusive charge transport dominated by long-range charge impurities, as reported in previous experiments on high-mobility devices[11,23] and expected theoretically.[29] The small departure from a T^2 dependence is expected as the samples are not exactly at the Dirac point. We conclude that all samples are in the diffusive regime at low charge density [Fig. 2(b) and SM, Sec. 3] and scattering is predominantly due to charged impurities. The data in Fig. 2(a), and its agreement with theory, serves as a reliable thermometer for T_e in our devices.

After establishing the T_e thermometry, we demonstrate controlled Joule self-heating of the electrons to apply a thermal bias $\Delta T = T_e - T$ between the suspended graphene and the electrodes. Figure 3(a) shows R vs V_B for sample A at $T = 50$, 100, 150 K (for samples B and C, see Figs. S3 and S4). Figure 3(b) shows the details of the data at 100 K. R decreases monotonically with increasing V_B, at all T. We argue that this change in the R vs V_B data is caused by Joule heating of the sample. Other mechanisms which could cause a nonlinear I-V_B relation include scattering from flexural phonons, in-plane optical phonons, substrate phonons, and Zener-Klein tunneling. We restrict our measurements to $V_B \lesssim 30$ meV. This rules out any R change due to scattering from optical in-plane phonons, ≈ 200 meV, and flexural phonons, ≈ 70 meV, in graphene.[11] Phonons in the substrate can also be ruled out
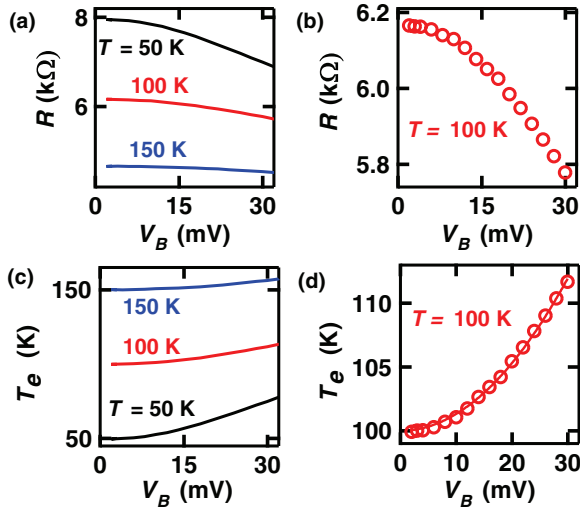
FIG. 3. (Color online) Electron heating. (a) R vs V_B at various T for device A at $V_G = 0.5$ V $\approx V_D$. (b) Details of the data at $T = 100$ K. Joule heating due to V_B raises the flake's average T_e above T. T_e is extracted using Fig. 2(a). (c) and (d) show T_e vs V_B in sample A at a few different T, and at $T = 100$ K, respectively.

as the samples are suspended. The contribution of Zener-Klein tunneling to I-V_B nonlinearity was only observed in very low-mobility devices, and at $V_B > 100$ mV.[30] This leaves Joule heating as the only plausible cause for the observed R vs V_B behavior.[31] Using the calibration curve for the samples, Fig. 2(a), and data from Figs. 3(a) and 3(b), we extract the average T_e vs V_B, as shown for sample A in Figs. 3(c) and 3(d). In Fig. 3(d), we fit a power law (solid line) $T_e = 100 + B V_B^x$, and find $x = 2.00 \pm 0.04$, as expected for Joule heating over a small T_e range, where K_e and R do not change appreciably (samples B and C, SM, Sec. 4). Figures 3(d), S3(d), and S4(d) show that the accuracy with which T_e can be extracted is much better than 1 K. We calculate T_e errors from the scatter of the data in Fig. 3(d), and similar plots at each T, to vary from 0.2 K [steepest regions of Fig. 2(a)] up to 2 K [flat regions of Fig. 2(a)]. The smooth dependence of T_e on V_B at all T is consistent with electrons having a well defined temperature, as predicted by calculations of the e-e collision length[32] (SM, Sec. 5). This is also confirmed by the K_e data shown below.

Since our devices are much wider than the elastic mean free path (SM, Sec. 3), the effect of their edges on transport should be small. We use a one-dimensional heat equation to extract K_e in our devices, $K_e \frac{d^2 T_e}{dx^2} + Q = 0$, where $Q = R I^2 / W L h$ is the Joule heating power per unit volume, W the width, L the length, and $h = 0.335$ nm the thickness. Using boundary conditions $T_e = T$ at the two ends (contacts) of the flake, we find $T_e(x) = T + (LQx - Qx^2)/2K_e$. Averaging over the length we find, $T_e = (1/L) \int_0^L T_e(x) dx = T + (QL^2)/(12K_e)$. Finally, $K_e = \frac{QL^2}{12\Delta T}$, where $\Delta T = T_e - T$. Using R and I from Fig. 3 and similar plots, for $\Delta T = 1$, 2, and 5 K we extract K_e vs T_e in Fig. 4(a) for sample A. Figure 4(b) shows K_e vs T_e for all three samples for $\Delta T = 5$ K. Data in Fig. 4 show a strong K_e dependence on T_e ranging from roughly 0.5 W/K m at 20 K to 11 W/K m at 300 K. The T_e range
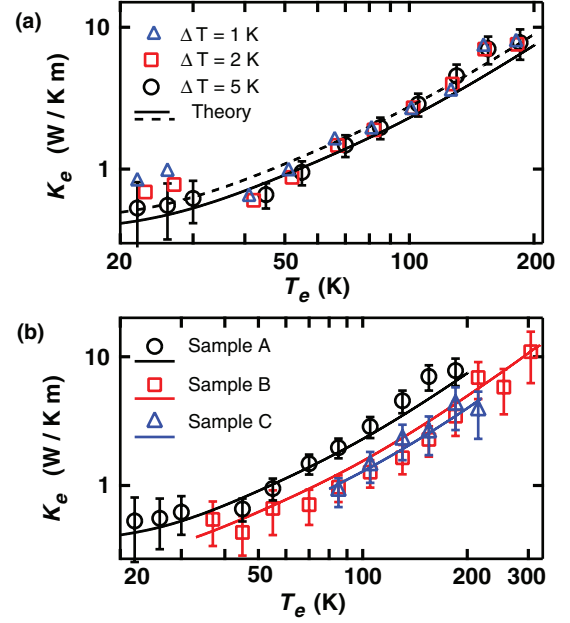

FIG. 4. (Color online) Electronic thermal conductivity K_e in the quasi-intrinsic regime, $n_{\text{tot},T=0} \approx 1.7 \times 10^{10}$ cm^{-2} (samples A and B) and 2.1×10^{10} cm^{-2} (sample C). (a) K_e vs T_e for $\Delta T = T_e - T = 1$, 2, and 5 K for sample A. The solid line is a theoretical calculation of $K_{e\text{-th}}$. The dashed line shows the same calculation with a contact resistance $R_c = R_{o-\text{Dirac}}$. The error bars are shown for the $\Delta T = 5$ K data. (b) K_e vs T_e for $\Delta T = 5$ K for samples A, B and C, and $K_{e\text{-th}}$ for each sample.

is limited to the region where we have accurate thermometry [Fig. 2(a)], up to ≈ 200 K for A and C, and 300 K for B. Error bars representing the total uncertainty on K_e are shown for the $\Delta T = 5$ K data (see SM, Sec. 6). If the V_B needed to apply ΔT were to dope significantly the samples, it could affect the measured K_e. Using $n_{\text{tot}}(T)$ (SM, Sec. 3),[33] we define an effective chemical potential $\mu_{\text{eff}}(T) = \hbar v_F \sqrt{\pi n_{\text{tot}}(T)}$. For instance, at $T = 100$ K, $\mu_{\text{eff}}(100 \text{ K}) = 18$, 18.4, and 19.5 meV, respectively, for the three devices. The V_B necessary to achieve $\Delta T \leqslant 5$ K in Fig. 4 is always smaller than $\mu_{\text{eff}}(T)$. We only observe a change in the extracted K_e values when ΔT exceeds 8 K, and $V_B > \mu_{\text{eff}}(T)$. Thus V_B does not affect our K_e, with the caveat that we cannot extract K_e precisely at $n = 0$. The thermoelectric voltages in our devices are negligible compared to V_B.[34,35]

We compare our data with the usual model for diffusing particles in two dimensions, $K_{e\text{-th}} = \frac{1}{2} C v l$. If the heat flow is due to charge carriers, then the specific heat is $C = C_e$, the velocity is $v_F = 10^6$ m/s, and the mean free path l is the same as for charge transport. We find (SM, Sec. 3), $l_{\text{A-avg}}$, $l_{\text{B-avg}}$, and $l_{\text{C-avg}} = 71(85)$, 47(59), and 37(51) nm on average over the T_e range with $R_c = 0$ ($R_{o-\text{Dirac}}$). We calculate C_e using the density of states for graphene and the Fermi-Dirac distribution (SM, Sec. 7). We plot $K_{e\text{-th}}$ in Figs. 4(a) and 4(b) as solid lines with $R_c = 0$. They capture the quantitative T_e dependence of our K_e data. The K_e data points are in good quantitative agreement with the calculated values for all three samples, and especially for samples A and C. The dashed line in Fig. 4(a) shows $K_{e\text{-th}}$ if we use $R_c = R_{o-\text{Dirac}}$. If we account

for R_c, i.e., smaller Q, K_e changes by the same magnitude as $K_{e\text{-th}}$ but in the opposite direction (not shown for clarity). The quantitative agreement between data and theory is not as accurate for sample B since its R is smaller than for samples A and C, and the impact of R_c could be bigger. The data and calculations shown in Fig. 4(b) with $R_c = 0$ are within 20%, 30%, and 15% of each other for samples A, B, and C. If we include $R_c = R_o$, which overestimates the effect due to R_c, the agreement between the data and theory for sample B is at worst within a factor of 2, and much better for samples A and C. We fit a power law expression $K_e \propto T^p$ over $T_e =$ 45–185 K for samples A and B, and find $p = 1.73 \pm 0.15$ and 1.63 ± 0.13, which is very close to the fit on $K_{e\text{-th}}$, $p_{\text{th}} =$ 1.62 and 1.59. This agreement is preserved even if we let $R_c = R_o$. As expected, p_{th} goes to 2 when $\mu/kT \ll 1$. We conclude that the K_e data is consistent with heat being carried by particles moving with the v_F and l of the charge carriers. The magnitude of K_e reaches ≈ 11 W/K m at 300 K with $n_{\text{tot},T=0} \approx$ 1.7–2.1×10^{10} cm^{-2}.

A condition to make reliable K_e measurements is that all of the Joule heat remains in the carriers until they diffuse to the leads. Both experiments and theory confirm that the electron-phonon energy transfer in high-mobility graphene, at low V_B, is very small below 300 K,[13,14,29,31] and decreases at lower T and n. In our devices, we extract a cooling length for hot electrons (SM, Sec. 8), $\xi \approx 100$–10 μm for $T_e = 20$–300 K. Since ξ is much longer than L, and V_B below the energy of optical phonons, we expect T_e and T to be decoupled in our devices when $V_B \neq 0$, and all of the Joule heat to be carried to the contacts by charge carriers. Indeed, the K_e we measure are two to three orders of magnitude lower than the reported phonon thermal conductivity K_p in graphene.[19,20]

In summary, we fabricated high quality suspended graphene devices, developed self-thermometry and self-heating methods to extract and control T_e, and the electronic thermal conductivity in graphene. We extracted K_e in the quasi-intrinsic regime, $n_{\text{tot},T=0} \approx 1.7$–$2.1 \times 10^{10}$ cm^{-2}, from $T_e = 20$ to 300 K. The K_e data in three different devices are in very good agreement with a model where heat is carried by diffusing Dirac quasiparticles. Our results provide evidence that the dominant electron cooling mechanism in intrinsic submicron graphene devices below 300 K is hot-electron diffusion to the leads. The theoretical model we use naturally leads to the Wiedemann-Franz relation in the doped regime and suggests that it should be obeyed in graphene.

*a.champagne@concordia.ca

[1]S. Z. Butler, S. M. Hollen, L. Y. Cao, Y. Cui, J. A. Gupta, H. R. Gutierrez, T. F. Heinz, S. S. Hong, J. X. Huang, A. F. Ismach, E. Johnston-Halperin, M. Kuno, V. V. Plashnitsa, R. D. Robinson, R. S. Ruoff, S. Salahuddin, J. Shan, L. Shi, M. G. Spencer, M. Terrones, W. Windl, and J. E. Goldberger, ACS Nano **7**, 2898 (2013).

[2]R. Bistritzer and A. H. MacDonald, Phys. Rev. Lett. **102**, 206410 (2009).

[3]W. K. Tse and S. Das Sarma, Phys. Rev. B **79**, 235406 (2009).

[4]S. S. Kubakaddi, Phys. Rev. B **79**, 075417 (2009).

[5]S. Berciaud, M. Y. Han, K. F. Mak, L. E. Brus, P. Kim, and T. F. Heinz, Phys. Rev. Lett. **104**, 227401 (2010).

[6]D. K. Efetov and P. Kim, Phys. Rev. Lett. **105**, 256805 (2010).

[7]J. C. W. Song, M. Y. Reizer, and L. S. Levitov, Phys. Rev. Lett. **109**, 106602 (2012).

[8]A. C. Betz, F. Vialla, D. Brunel, C. Voisin, M. Picher, A. Cavanna, A. Madouri, G. Feve, J. M. Berroir, B. Placais, and E. Pallecchi, Phys. Rev. Lett. **109**, 056805 (2012).

[9]A. C. Betz, S. H. Jhang, E. Pallecchi, R. Feirrera, G. Feve, J. M. Berroir, and B. Placais, Nat. Phys. **9**, 109 (2013).

[10]M. W. Graham, S. F. Shi, D. C. Ralph, J. Park, and P. L. McEuen, Nat. Phys. **9**, 103 (2013).

[11]S. Das Sarma, S. Adam, E. H. Hwang, and E. Rossi, Rev. Mod. Phys. **83**, 407 (2011).

[12]K. Saito, J. Nakamura, and A. Natori, Phys. Rev. B **76**, 115409 (2007).

[13]N. M. Gabor, J. C. W. Song, Q. Ma, N. L. Nair, T. Taychatanapat, K. Watanabe, T. Taniguchi, L. S. Levitov, and P. Jarillo-Herrero, Science **334**, 648 (2011).

[14]J. C. W. Song, M. S. Rudner, C. M. Marcus, and L. S. Levitov, Nano Lett. **11**, 4688 (2011).

[15]S. Ghosh, I. Calizo, D. Teweldebrhan, E. P. Pokatilov, D. L. Nika, A. A. Balandin, W. Bao, F. Miao, and C. N. Lau, Appl. Phys. Lett. **92**, 151911 (2008).

[16]M. Freitag, M. Steiner, Y. Martin, V. Perebeinos, Z. H. Chen, J. C. Tsang, and P. Avouris, Nano Lett. **9**, 1883 (2009).

[17]J. H. Seol, I. Jo, A. L. Moore, L. Lindsay, Z. H. Aitken, M. T. Pettes, X. S. Li, Z. Yao, R. Huang, D. Broido, N. Mingo, R. S. Ruoff, and L. Shi, Science **328**, 213 (2010).

[18]I. Jo, I. K. Hsu, Y. J. Lee, M. M. Sadeghi, S. Kim, S. Cronin, E. Tutuc, S. K. Banerjee, Z. Yao, and L. Shi, Nano Lett. **11**, 85 (2011).

[19]A. A. Balandin, Nat. Mater. **10**, 569 (2011).

[20]E. Pop, V. Varshney, and A. K. Roy, MRS Bull. **37**, 1273 (2012).

[21]V. E. Dorgan, A. Behnam, H. J. Conley, K. I. Bolotin, and E. Pop, Nano Lett., doi:10.1021/nl400197w (2013).

[22]See Supplemental Material at http://link.aps.org/supplemental/10.1103/PhysRevB.87.241411 for images of sample C, data on and discussion of the contact resistance and mean free path, self-heating data in samples B and C, electron-electron scattering length, error analysis, specific heat calculations, and electron cooling length estimate.

[23]K. I. Bolotin, K. J. Sikes, Z. Jiang, M. Klima, G. Fudenberg, J. Hone, P. Kim, and H. L. Stormer, Solid State Commun. **146**, 351 (2008).

[24]X. Du, I. Skachko, A. Barker, and E. Y. Andrei, Nat. Nanotechnol. **3**, 491 (2008).

[25] E. V. Castro, H. Ochoa, M. I. Katsnelson, R. V. Gorbachev, D. C. Elias, K. S. Novoselov, A. K. Geim, and F. Guinea, Phys. Rev. Lett. **105**, 266601 (2010).

[26] In the doped regime (away from the Dirac point) and at low temperature, the R vs T data for sample B are consistent with ballistic electron transport. These data will be discussed in a future publication.

[27] Y. K. Koh, M. H. Bae, D. G. Cahill, and E. Pop, Nano Lett. **10**, 4363 (2010).

[28] M. Muller, M. Brauninger, and B. Trauzettel, Phys. Rev. Lett. **103**, 196801 (2009).

[29] S. Das Sarma and E. H. Hwang, Phys. Rev. B **87**, 035415 (2013).

[30] N. Vandecasteele, A. Barreiro, M. Lazzeri, A. Bachtold, and F. Mauri, Phys. Rev. B **82**, 045416 (2010).

[31] J. K. Viljas, A. Fay, M. Wiesner, and P. J. Hakonen, Phys. Rev. B **83**, 205421 (2011).

[32] Q. Li and S. Das Sarma, Phys. Rev. B **87**, 085406 (2013).

[33] V. E. Dorgan, M. H. Bae, and E. Pop, Appl. Phys. Lett. **97**, 082112 (2010).

[34] Y. M. Zuev, W. Chang, and P. Kim, Phys. Rev. Lett. **102**, 096807 (2009).

[35] E. H. Hwang, E. Rossi, and S. Das Sarma, Phys. Rev. B **80**, 235415 (2009).